ORIGINAL ARTICLE

Development and analysis of patient-derived xenograft mouse models in intravascular large B-cell lymphoma

K Shimada[1,2], S Shimada[3], K Sugimoto[2,4], M Nakatochi[5], M Suguro[6], A Hirakawa[5], TD Hocking[7], I Takeuchi[8], T Tokunaga[2,9], Y Takagi[2], A Sakamoto[2], T Aoki[2], T Naoe[2,9], S Nakamura[3], F Hayakawa[2], M Seto[6,10], A Tomita[2] and H Kiyoi[2]

Intravascular large B-cell lymphoma (IVLBCL) is a distinct disease entity with the peculiar characteristic that tumor cells proliferate within vessels. Despite recent advances in understanding the disease from clinical aspects, the underlying pathogenesis remains unknown. Here we demonstrate analyses of IVLBCL biology using four xenograft mouse models established from primary IVLBCL samples. In all four models, the main characteristic of IVLBCL tumor cell proliferation within vessels was retained. Time-lapse engraftment analyses revealed that the tumor cells initially engrafted and proliferated in the sinusoids and vessels in the liver and then engrafted and proliferated in multiple organs. Intriguingly, serial passage of tumor cells from the adrenal gland of a transplanted mouse developed from primary patient bone marrow cells into a second mouse showed that the tumor cells mainly distributed into the adrenal gland in the second mouse, implying the existence of clonal selection and/or evolution at engraftment of a specific organ. Gene expression profiling analyses demonstrated that the gene set associated with cell migration was enriched for normal peripheral blood B cells, indicating that inhibition of cell migration might be involved in IVLBCL pathogenesis. In conclusion, the mouse xenograft models described here are essential tools for uncovering IVLBCL biology.

INTRODUCTION

Intravascular large B-cell lymphoma (IVLBCL) is a rare distinct disease entity of extranodal large B-cell lymphoma according to the current World Health Organization (WHO) classification.[1] This disease is characterized by the selective growth of tumor cells in the lumina of small vessels.[2] Peculiar characteristics of IVLBCL including the absence of remarkable lymphoadeno-pathy, and the presence of nonspecific clinical symptoms such as fever of unknown origin and general malaise, make precise diagnosis difficult. These difficulties result in a delay in timely diagnosis and initiation of treatment, and thus disease progression at diagnosis leads to poor prognosis.[3,4] Recent advances in understanding the disease and in diagnostic approaches including random skin biopsies have improved ante-mortem diagnostic yield.[5–7] Moreover, application of the anti-CD20 monoclonal antibody, rituximab, has resulted in improved clinical outcomes.[8–10]

Although there is apparent progress in its diagnosis and treatment, the fundamental question regarding IVLBCL, that is, why do the tumor cells proliferate in the lumina of vessels, remains unanswered. Previous reports suggested that the lack of CD29, CD54 and CD11a might be associated with the pathogenesis of IVLBCL; however, it has been difficult to validate these findings.[11,12] The most serious obstacle to uncovering the underlying biology of IVLBCL seem to be difficulty in obtaining a lot of live tumor cells from diagnostic specimens because of the specific characteristics of IVLBCL. This problem has made it very difficult to investigate disease mechanisms.

Recent studies using immunodeficient mice have led to the development of xenograft malignant lymphoma models from patient-derived tumor cells.[13,14] In these xenograft models using NOD/Shi-*scid* IL2Rγ[null] (NOG) mice,[13,15–17] it is possible to achieve successful engraftment and subsequent proliferation of primary lymphoma cells. If it was possible to develop a xenograft model from IVLBCL patient tumor cells, such a model might be a very powerful tool for uncovering the underlying biology of IVLBCL. Herein, we aimed to develop such xenograft models using primary IVLBCL samples and to use these models to investigate the underlying biology of IVLBCL.

MATERIALS AND METHODS

Development of xenograft models

To develop xenograft mouse models, 1.0×10^6–5.0×10^6 primary bone marrow (BM) mononuclear cells from patients clinically suspected or pathologically diagnosed with IVLBCL were basically transplanted intrave-nously into 2 NOG mice (purchased from the Central Institute for Experimental Animals, Tokyo, Japan). Written informed consent for the experimental use of patient BM cells was obtained before the BM aspiration. The protocol for the experimental use of patient samples was approved by the institutional review board of Nagoya University Hospital. To suppress the proliferation of human T cells from patient BM in NOG mice, 100 μg of OKT3, an anti-CD3 monoclonal antibody (Miltenyi Biotec GmbH, Bergisch Gladbach, Germany and BioLegend, San Diego, CA, USA),

[1]Institute for Advanced Research, Nagoya University, Nagoya, Japan; [2]Department of Hematology and Oncology, Nagoya University Graduate School of Medicine, Nagoya, Japan; [3]Department of Pathology and Clinical Laboratories, Nagoya University Hospital, Nagoya, Japan; [4]Fujii Memorial Research Institute, Otsuka Pharmaceutical Co., Ltd, Otsu, Japan; [5]Center for Advanced Medicine and Clinical Research, Nagoya University Graduate School of Medicine, Nagoya, Japan; [6]Division of Molecular Medicine, Aichi Cancer Center Research Institute, Nagoya, Japan; [7]Department of Human Genetics, McGill University, Montreal, Quebec, Canada; [8]Department of Computer Science/Scientific and Engineering Simulation, Nagoya Institute of Technology, Nagoya, Japan; [9]Department of Hematology, National Hospital Organization, Nagoya Medical Center, Nagoya, Japan and [10]Department of Pathology, Kurume University School of Medicine, Kurume, Japan. Correspondence: Dr K Shimada, Department of Hematology and Oncology, Nagoya University Graduate School of Medicine, 65 Tsurumai-cho, Showa-ku, Nagoya 4668550, Japan.
E-mail: kshimada@med.nagoya-u.ac.jp

was also injected intraperitoneally. Approximately 2 to 3 months after transplantation, the tumor-bearing mice (denoted F0) were killed. Engraftment of the lymphoma cells was investigated using flow cytometry (FCM) and pathological specimens. Leukocytosis in peripheral blood obtained from the inferior vena cava was also evaluated using FCM. In the case of engraftment, $1.0 \times 10^6 – 5.0 \times 10^6$ tumor cells from each organ of the mouse models were serially injected into other mice (using 2 mice per organ) (F1) intravenously or intraperitoneally. Mouse models were considered to be established based on the success of secondary serial passage of the tumors, that is, development of third-passage transplanted mice (F2). Patient-derived xenografted tumor cells obtained from F0 to F2 mice were used in the subsequent analyses. To confirm that the xenografted tumor cells were clonally related to the original tumors, the sequences of the variable region of the immunoglobulin heavy chain were analyzed based on BIOMED-2 guidelines (Invivoscribe, San Diego, CA, USA).[18] All the animal experimental procedures complied with the Regulations regarding Animal Experiments in Nagoya University.

Chimerism analysis of the tumor engrafted in each organ

To determine whether the tumor that arose in each organ was derived from the patient or not, the presence of human CD45- and mouse CD45-positive cells was investigated by FCM (FACSCalibur, BD, Franklin Lakes, NJ, USA) using the monoclonal antibodies listed in Supplementary Table S1. The percentage of hCD45-positive cells in the total CD45-positive mouse and human cells in each organ was defined as the chimerism of each organ.

Pathological analyses and immunohistochemical staining

Formalin-fixed, paraffin-embedded tissues of patient and mouse samples were evaluated by routine hematoxylin and eosin staining and immunohistochemistry using the primary antibodies listed in Supplementary Table S1. Hematopathologists (SS and SN) reviewed the existence of tumor cells in pathological specimens. The specimens were observed with an Olympus BX51 N-34 (Olympus, Tokyo, Japan), and the photos were taken with a Nikon DS-Fi1 (Nikon, Tokyo, Japan) and BZ-9000 (Keyence, Osaka, Japan).

Surface antigens and B-cell origin analyses of tumor cells

To evaluate surface antigens associated with cell adhesion and with the cell of origin as the normal counterpart of the tumor cells, FCM analyses were performed using the monoclonal antibodies described in Supplementary Table S1 (FACSCalibur and FACSCanto2, BD).

Time course engraftment analyses after transplantation

To investigate the pattern of engraftment and proliferation of the IVLBCL tumor cells in the mouse models, time-lapse engraftment analyses were performed. After intravenous injection of 5.0×10^6 tumor cells from a tumor formed in the spleen in mouse models (F2), the mice were killed according to a time course. Tumor engraftment and proliferation patterns were pathologically analyzed at time points of 1, 2, 3 and 4 weeks after inoculation.

Organ specificity of tumor engraftment in serial passages

To investigate whether there was any specificity associated with IVLBCL tumor cells engrafted in each organ, we serially transplanted 1.0×10^6 tumor cells from each organ of the first transplanted mouse (F0), which was developed from the primary BM sample, into a second mouse (F1). When tumors appeared in the second mouse, the pattern of tumor formation and the chimerism in each organ was analyzed. In particular, we analyzed the organ specificity of tumor cells engrafted in the BM, liver and adrenal gland in the first transplanted mouse (F0).

Dependency of tumor cells on vascular endothelial cells

To analyze the dependency of the tumor cells on vascular endothelial cells, we evaluated tumor cell survival under co-culture with or without human umbilical vein endothelial cells (HUVECs; purchased from Takara Bio Inc., Shiga, Japan). In brief, 5.0×10^5 IVLBCL tumor cells from a tumor formed in the spleen in mouse models (F2) were placed into a 6-well plate coated with HUVECs or with cells of the BLS4 mouse fibroblast reticular cell line[19] (kindly provided by Dr Tomoya Katakai, Niigata University, Niigata, Japan).

After 24 h, the survival of cells co-cultured with or without HUVECs or BLS4 were analyzed. EBM-2 (Takara) supplemented with 2% fetal bovine serum and other supplements (EGM-2 bullet kit; Takara) was used as the culture medium for HUVECs. RPMI-1640 (Sigma-Aldrich, St Louis, MO, USA) supplemented with 10% fetal bovine serum (Gibco in Thermo Fisher Scientific, Waltham, MA, USA) was used for BLS4. Cell survival was evaluated by Trypan blue staining and by FCM of cells stained with anti-hCD20 (BioLegend) and 2 µg/ml of propidium iodide. The relative cell survival ratio was calculated by comparison of the cell survival rate at the initiation with that at the end of co-culture.

Array CGH analysis and genomic copy number PCR assay

To investigate genomic copy number alteration of IVLBCL tumor cells, array comparative genomic hybridization (CGH) analyses[20] were performed. In brief, genomic DNA was extracted from IVLBCL tumor cells from each mouse (F0 to F2) using the QIAamp DNA Blood Mini Kit according to the manufacturer's protocol (QIAGEN, Venlo, The Netherlands). Tumor genomic DNA was analyzed using the SurePrint G3 Human CGH Microarray Kit and Genomic Workbench (Agilent Technologies, Santa Clara, CA, USA). Pooled DNA from healthy volunteer donors was used as a reference. The background biases in the log2 ratio values of the CGH analysis data were adjusted according to standard statistical methods. Specifically, the correlation bias with guanine-cytosine content of the corresponding clone sequence was first removed. Subsequently, the probe-specific bias was also removed, where the bias at each probe was estimated by the running mean of the adjacent 10 probes in both slides. Copy number variations/polymorphisms were identified using a Database of Genomic Variants (http://projects.tcag.ca/variation/) and were then excluded from further analyses. Genomic copy number alterations in array CGH data were defined by interactively updating and labeling a maximum likelihood segmentation model using SegAnnDB software.[21] Subsequently, a genomic copy number assay was performed to validate the array CGH data. Genomic copy number located on persistent alterations loci was evaluated by real-time PCR according to the manufacturer's protocol (TaqMan Copy Number Assay, Applied Biosystems in Thermo Fisher Scientific), and the data were analyzed using CopyCaller software (Applied Biosystems in Thermo Fisher Scientific). Array CGH data are available at the Gene Expression Omunibus database under accession number GSE72028.

Gene expression profiling analysis

To evaluate gene expression profiling (GEP) of IVLBCL tumor cells, tumor cells from a tumor formed in the spleen of mouse models (F2) and peripheral blood mononuclear cells from healthy volunteer donors used as normal controls were purified by magnetic beads selection targeting the CD19 antigen (Miltenyi Biotec). Total RNA of CD19-positive cells was extracted using TRIzol solution (Thermo Fisher Scientific). RNA concentrations and purities were determined by measurement of A260, A260/A280 and A260/A230 ratios using a NanoDrop-1000 Spectrophotometer (Thermo Fisher Scientific) and these qualities were confirmed using the Agilent 2100 Bioanalyzer (Agilent Technologies). RNA samples with high integrity (RNA integrity number score $\geqslant 9.0$) were evaluated for GEP analyses using the SurePrint G3 Human Gene Expression $8 \times 60K$ v2 Microarray Kit (Agilent Technologies). Microarray slides were scanned using the Agilent DNA Microarray Scanner. The GEP analyses described above were performed by Oncomics Co. Ltd (Nagoya, Japan). Subsequently, expression levels of transcripts were normalized to the 75th percentile using GeneSpring version 13.0 (Agilent Technologies), and were log2 transformed. Out of 50 599 probes measured in this microarray, probes detected in all 8 samples were selected, and a total of 19 019 probes remained for further analysis.

To confirm the similarity among the eight samples, principal component analysis and hierarchical clustering were performed. Principal component analysis was performed using the prcomp function with the scaling option on in the R software version 3.2.1 (https://www.r-project.org/). The CLUSTER program was used to perform average linkage hierarchical clustering, using mean centering for normalization and an uncentered correlation coefficient, and the results were displayed using TREEVIEW (http://jtreeview.sourceforge.net).[22] The gene expression levels of IVLBCL tumor cells and normal control B cells were compared by using the significance analysis of microarrays method.[23] The same microarray data

Table 1. Patient characteristics

Characteristic	1	2	3	4
Age	59	72	77	76
Sex (M/F)	M	M	M	F
PS	2	2	2	4
LDH (U/l)	2440	717	2498	693
Clinical stage	IV	IV	IV	IV
IPI	High	High	High	High
Presence of B symptom	−	+	+	+
Hepatomegaly	+	+	−	−
Splenomegaly	+	+	+	−
Respiratory symptom	−	−	−	+
Neurologic symptom	−	−	−	+
Skin involvement	−	−	+	+
Hemophagocytosis	−	+	+	+
Tumor cells in PB	3%	−	3%	−
WBC (/μl)	12 100	5200	11 700	7600
Hemoglobin (g/dl)	6.8	8.5	11.7	8.5
Platelet count ($\times 10^4$/μl)	4.5	2.1	5.6	5.2
Albumin (g/dl)	2.5	2.8	2.9	1.7
Bilirubin (mg/dl)	1.0	2.0	0.6	0.8
Creatinine (mg/dl)	0.6	0.67	0.76	0.61
CRP (mg/dl)	14.78	7.16	7.27	8.57
sIL-2R (U/ml)	4130	26 800	6400	8160
AIVL[a]	No	Yes	Yes	Yes
Initial treatment	R-CHOP+R-HDMTX	−	R-CHOP+R-HDMTX	R-CHOP+R-HDMTX
Antitumor response	PD	NE	CR	CR
Prognosis	Alive	DOD	Alive	DOD

Abbreviations: AIVL, Asian-variant intravascular large B-cell lymphoma; CHOP, cyclophosphamide, doxorubicin, vincristine, prednisolone; CR, complete response; CRP, C-reactive protein; DOD, died of disease; F, female; HDMTX, high-dose methotrexate; IPI, International Prognostic Index; LDH, lactate dehydrogenase; M, male; NE, not evaluable; PB, peripheral blood; PD, progressive disease; PS, performance status; R, rituximab; sIL-2R, soluble interleukin-2 receptor; WBC, white blood cell count. [a]The criteria of an Asian variant of intravascular large B-cell lymphoma (IVLBCL) previously defined by Murase et al.[25] were as follows: (1) at least two of three of the following clinical and laboratory criteria: cytopenia (hemoglobin 11 g/dl or red blood cell count (RBC) 350×10^4/μl and/or platelet count 10×10^4/μl); hepatomegaly and/or splenomegaly; absence of overt lymphadenopathy and tumor formation; and (2) all three of the following histopathologic criteria: erythrocyte hemophagocytosis; immunophenotypic evidence of proliferating neoplastic B cells with large-cell morphology; pathologic findings of intravascular proliferation and/or sinusoidal involvement of lymphoma cells.
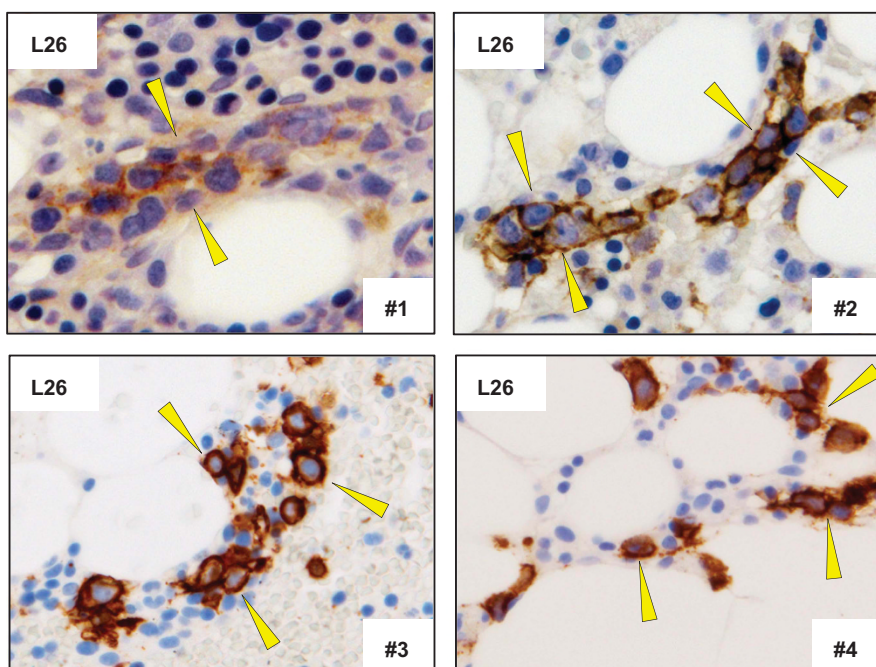

Figure 1. Pathological specimens of bone marrow samples of IVLBCL patients from whom the xenograft models originated. L26 immunostaining of CD20-positive cells in bone marrow cells of the four IVLBCL patients. CD20-positive tumor cells proliferate in line with sinusoidal patterns, as indicated by yellow arrowheads. Original magnification ×400, Olympus BX51 N-34.
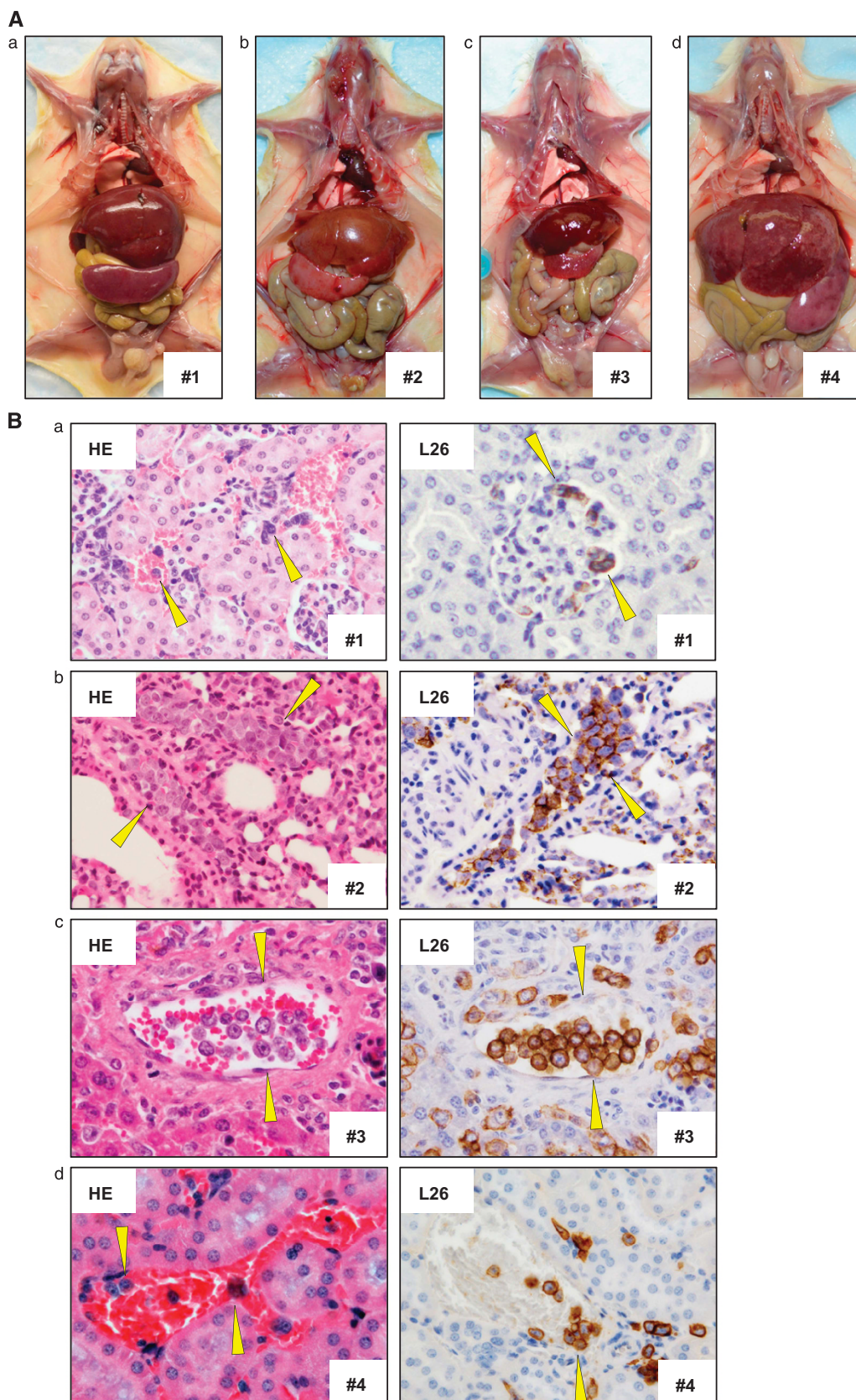
Figure 2. Autopsy findings and pathological specimens of IVLBCL xenograft models. (**A**) Autopsy findings of the mouse models that developed tumors are shown. The numbers of the mouse models match those of the originating patients shown in Figure 1. (**B**) Hematoxylin and eosin (HE)-stained (left panels) and L26 immunostained (right panels) pathological specimens of each mouse model are shown. The specimens are of kidney from mouse 1 (a), lung from mouse 2 (b), liver from mouse 3 (c) and kidney from mouse 4 (d). Tumor cells lodging within the vessels or sinusoids were observed in all four mouse models (yellow arrowheads). Original magnification ×400, Olympus BX51 N-34.

sets were also analyzed using gene set enrichment analysis (GSEA).[24] Signal-to-noise and 1000 permutations of the genes were applied in the GSEA analysis with the gene sets obtained from the MSigDB database v5.

0.[24] A false discovery rate value of < 0.05 was considered significant for GSEA analysis. GEP data are also available at the Gene Expression Omunibus database under accession number GSE72028.
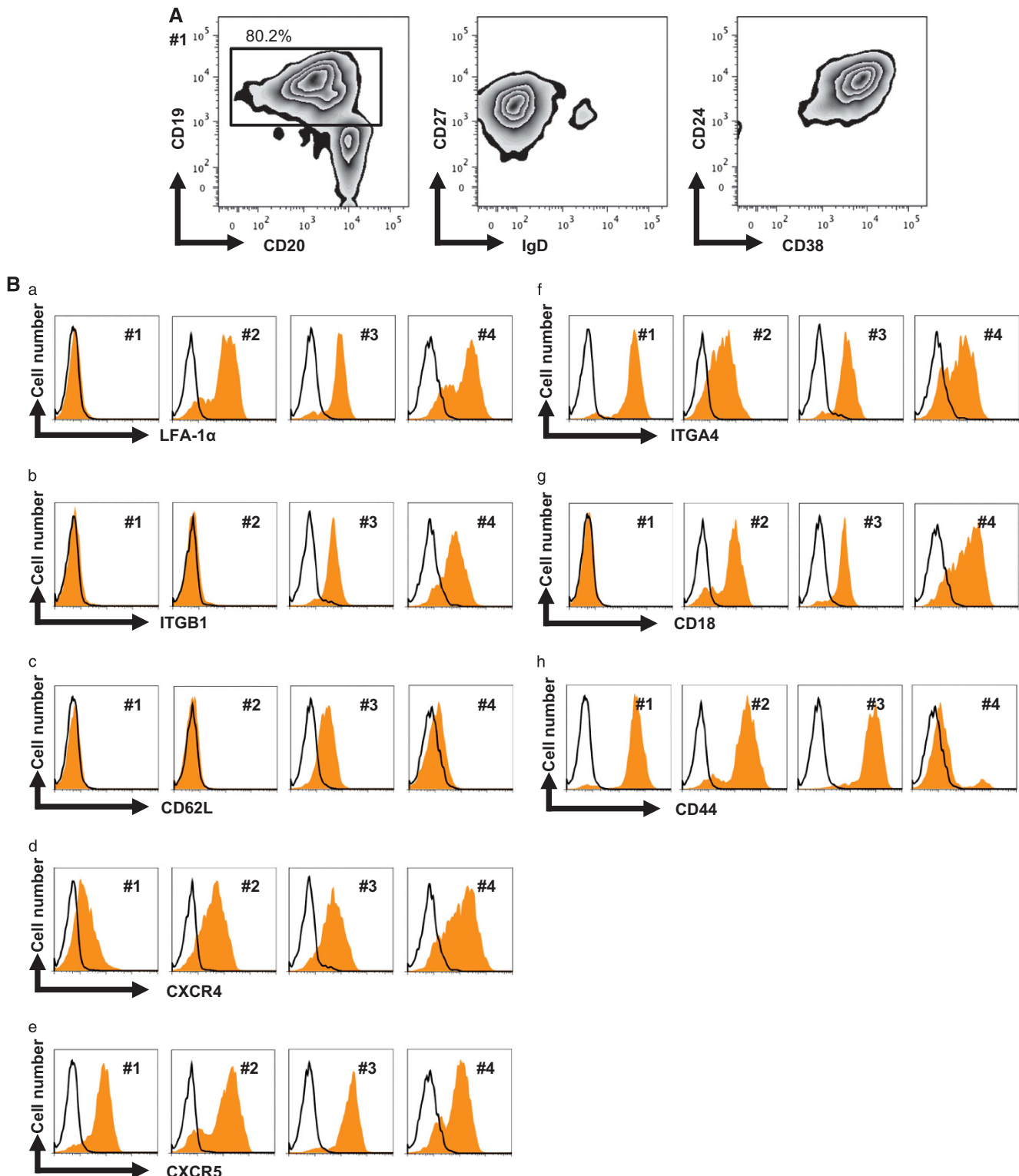
Figure 3. Expression of surface antigens relevant to a B-cell origin and of adhesion molecules. (**A**) The surface expression of the indicated molecules on the tumor cells from a tumor formed in the spleen of each mouse model was evaluated using FCM. The plot of mouse model 1 is shown. Human CD19-PerCP-Cy5.5$^+$ and CD20-APC-Cy7$^+$ B cells with a CD27-PE-Cy7$^+$, IgD-FITC$^-$, CD24-PE$^+$ and CD38-APC$^+$ phenotype is consistent with a memory B-cell phenotype. (**B**) The expression of representative adhesion molecules was analyzed by FCM using anti- LFA-1α-FITC (a), ITGB1-PE (b), CD62L-FITC (c), CXCR4-PE (d), CXCR5-FITC (e), ITGA4-PE (f), CD18-FITC (g) and CD44-FITC (h) antibodies.

RESULTS

Characteristics of patients whose IVLBCL samples were used to establish mouse models

Bone marrow mononuclear cells from four patients diagnosed with IVLBCL were transplanted intravenously to develop mouse xenograft models. The characteristics of these four patients are shown in Table 1. High elevation of lactate dehydrogenase (693–2498 U/l) and soluble interleukin-2 receptor (4130–26800 U/l) was observed in all four patients. Clinical stage at diagnosis of all four patients was stage IV. Patient 1 was the only case in which
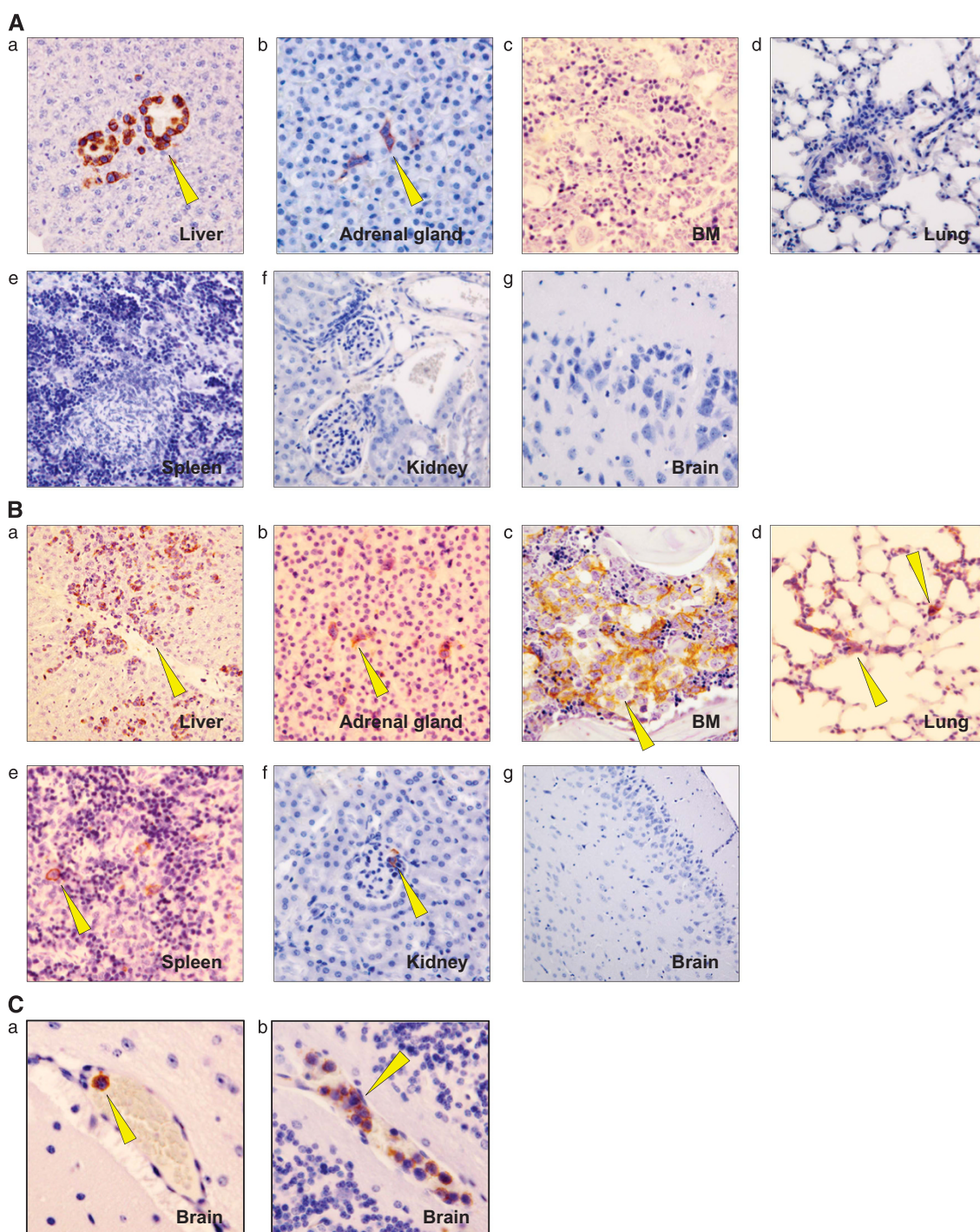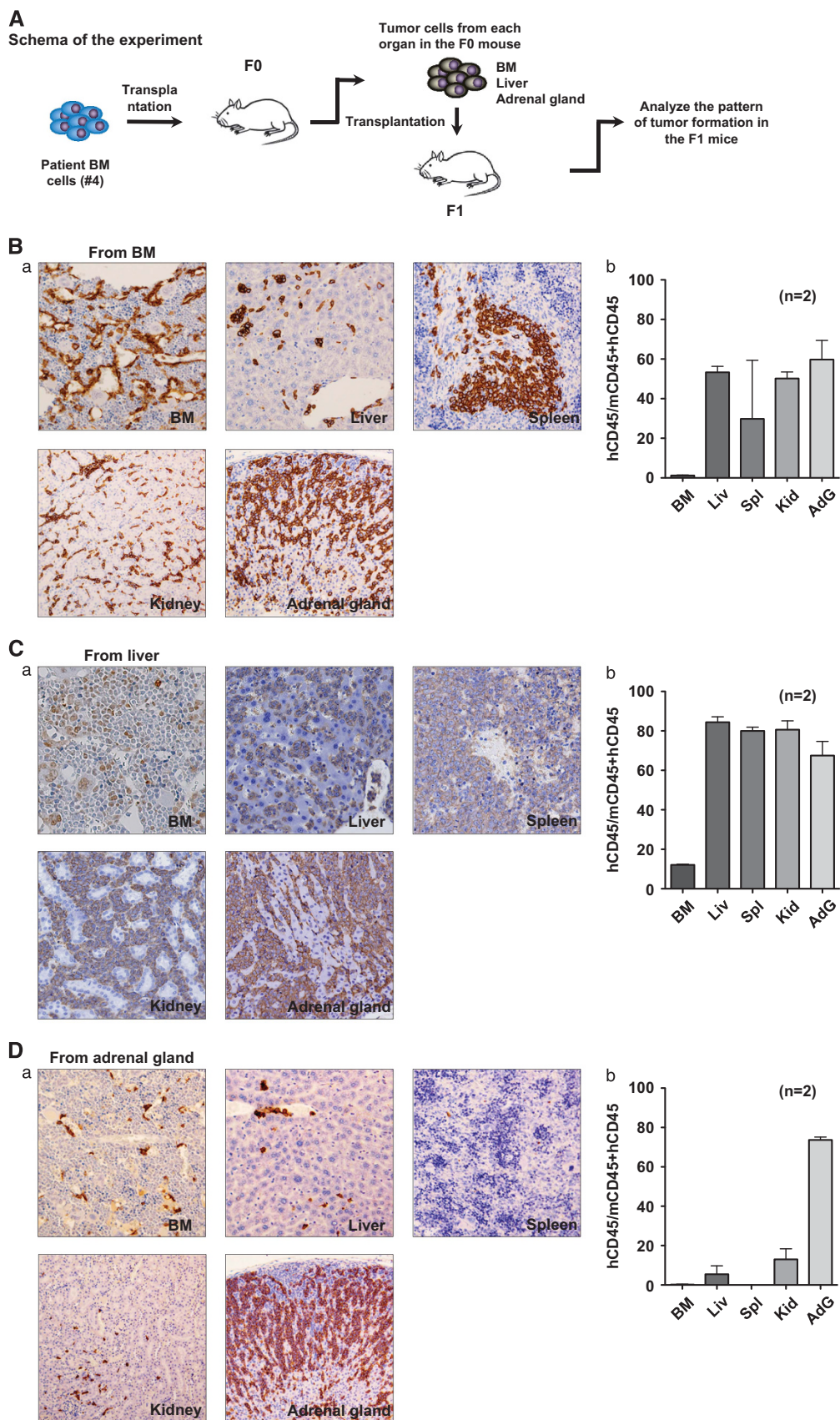
Figure 4. Time-lapse engraftment analysis of the tumor cells. (**A**) L26 immunostaining of pathological specimens of the mouse model 1 killed at 1 week after inoculation is shown. Tumor cells engrafted within the vessels and sinusoids of the liver (a) and adrenal gland (b) are highlighted by yellow arrowheads. At this time point, no tumor cells could be detected in the remaining organs including in the BM (c), lung (d), spleen (e), kidney (f) or brain (g). (**B**) L26 immunostaining of pathological specimens of the mouse model 1 killed at 2 weeks after inoculation is shown. Tumor cells are highlighted by yellow arrowheads, and were detected in multiple organs (a–f) except for the brain (g). Original magnification ×400, Olympus BX51 N-34. (**C**) L26 immunostaining of pathological specimens of the brain of mouse model 1, killed at 3 weeks (a) and 4 weeks (b) after inoculation is shown. Tumor cells, as highlighted by the yellow arrowhead, were detected in the brain at 3 weeks after inoculation. Original magnification ×400, Olympus BX51 N-34.

hemophagocytosis was not observed. The remaining three patients were classified into the Asian-variant IVLBCL.[25] Except for patient 2 who was not timely diagnosed, the remaining patients received rituximab-containing chemotherapies. Patients 1 and 3 are still alive, but patient 4 died of her disease after central nervous system relapse. All four patients were diagnosed with

A Schema of the experiment

B From BM

C From liver

D From adrenal gland

IVLBCL by pathological BM findings. Tumor cells proliferated in line with a sinusoidal pattern (Figure 1).

Development of mouse models and characteristics of the tumors

At 2 to 3 months after xenotransplantation of BM cells from all four patients, engraftment of the tumor was observed. The autopsy findings of the mouse models (1 to 4) established from each of the four patients are shown in Figure 2A. Hepatosplenomegaly was observed in all four mouse models. Pathological specimens stained with hematoxylin and eosin and L26 are shown in Figure 2B. Tumor cells were identified lodged in the lumina of vessels in the kidney, lung, liver and other organs in the mouse models. These data indicated that the main characteristic of the IVLBCL tumors was retained in the xenograft models. Even at the time of killing of mice because of disease progression, extensive leukocytosis by the tumor was not observed (Supplementary Figure S1). Subsequently, we determined whether the tumor cells from the mouse models were clonally related to those from the original patients. The sequence of the immunoglobulin heavy chain variable region of both the mouse models and the patient samples were analyzed, indicating that the tumor clone in the mouse models could be detected in the corresponding patient samples (Supplementary Figure S2). Immunophenotypes of the tumor cells of both the mouse models and the patient samples were also analyzed. Immunophenotypes of all four tumors was classified into the non-germinal center B cell type according to Hans' criteria,[26] and the phenotypes of the mouse models and patient samples were essentially the same (Supplementary Table S2). Moreover, we evaluated tumor cells from the mouse models in terms of characteristics of cell surface antigens associated with B-cell origin and cell adhesion molecules. The normal counterpart of IVLBCL has been postulated to be a transformed peripheral B cell.[1] As expected, tumor cells from all four mouse models displayed a $CD19^+$, $CD20^+$, $CD27^+$, IgD^-, $CD24^+$ and $CD38^+$ phenotype, indicating that IVLBCL tumor cells in these models originated from memory B cells (Figure 3A). Expression of cell adhesion molecules was evaluated as these molecules were previously suggested to have an association with the underlying pathogenesis of IVLBCL. Although the expression of CD29 (ITGB1) and CD11a (LFA-1α) was reported to be related with IVLBCL pathogenesis, consistent expression of these adhesion molecules was not observed in the tumor cells of the present analysis. In terms of the remaining antigens, we could not find any specific expression that might reflect the underlying biology of IVLBCL (Figure 3B).

Time-lapse engraftment analysis of the IVLBCL tumors

The proliferation and dissemination patterns of IVLBCL tumor cells, that is, how the tumor cells proliferate at one or multiple organs, and how the tumor cells systemically disseminate after engraftment, remain unknown. We therefore analyzed tumor engraftment and proliferation in the mouse models over a time course. At 1 week after intravenous inoculation of tumor cells from a tumor formed in the spleen in established mouse models, engraftment and proliferation of tumor cells were observed within vessels and sinusoids of the liver (Figure 4Aa and Supplementary Figure S3Aa and c). In mouse models 1 and 3, tumor cells were also engrafted in the adrenal gland (Figure 4Ab and Supplementary Figure S3C). Tumor cells were not detected in the BM or the spleen (Figure 4Ac and e and Supplementary Figure S3Aa and c). At 2 weeks after inoculation of the tumor cells, tumor engraftment and proliferation were observed in multiple organs except for the brain (Figure 4B and Supplementary Figure S3B and D). Tumor cells were found in the brain by 4 weeks after inoculation (Figure 4C and Supplementary Figure S3E). The combined data suggest that, at least in these models, the tumor cells were initially engrafted in the liver and then systemically disseminated and began to proliferate in multiple organs at an early phase after tumor transplantation. Tumor distribution after transplantation did not differ between intravenous and intraperitoneal injection (Supplementary Figure S4).

Specificity of tumor cells engrafted in the adrenal gland and in vitro dependency on vascular endothelial cells

To investigate whether there was any specificity in terms of tumor cell engraftment into a certain organ, we serially transplanted tumor cells engrafted in each organ in the first transplanted mouse into a second transplanted mouse (Figure 5A). As shown in Figures 5B and C, tumor cells that were engrafted into the BM and liver of the first transplanted mouse, which was developed from primary patient 4 BM cells, were distributed into systemic organs in the second transplanted mouse. On the other hand, tumor cells engrafted into the adrenal gland in the first transplanted mouse mainly formed a tumorous lesion in the adrenal gland in the second transplanted mouse. The chimerism of the adrenal gland was apparently higher than that of other organs (Figure 5D). We further investigated whether vascular endothelial cells supported the survival of the tumor cells in vitro. Tumor cells from a tumor formed in the spleen in the mouse model 1 were co-cultured with HUVECs, and tumor cell survival was evaluated 24 h after initiation of the co-culture. HUVECs supported the survival of the tumor cells in vitro (cell viability with HUVECs vs without HUVECs, 84.5% vs 8.6%; $P < 0.01$; Figure 6). In contrast, BLS4 cells, which are stromal cells in the lymph node, did not support tumor survival in co-culture (cell viability with BLS4 vs without BLS4, 28.8% vs 41.6%; $P = 0.04$; Supplementary Figure S5). We also performed the same experiments using tumor cells from mouse models 2 and 4; however, we could not detect an apparent effect of co-cultured cells on tumor survival in vitro because of the fragility of these tumor cells (data not shown).

Suppression of the genes associated with cell migration of IVLBCL cells

We performed array CGH and GEP analyses using tumor cells from mice 1 to 4 to investigate the presence of disease-specific

Figure 5. Serial passage of tumor cells engrafted in each organ. (**A**) The scheme of the experiment is shown. Tumor cells engrafted in the BM, liver and adrenal gland in the first transplanted mouse were serially transplanted into a second transplanted mouse. (**B**) L26 immunostaining of CD20-positive cells in pathological specimens of a mouse that was serially inoculated with tumor cells from the BM of the first transplanted mouse. The mice were killed on day 63 and on day 83 after transplantation. (a) The images shown are from a mouse killed on day 63. Original magnification ×100, Olympus BX51 N-34. The human/mouse chimerism of each organ was determined by analysis of human and mouse CD45 (b). (**C**) As described for (**B**), except that the mouse was inoculated with tumor cells from the liver and was killed on day 82 after transplantation. Original magnification ×200, Keyence BZ-9000. (**D**) L26 immunostaining of CD20-positive tumor cells in pathological specimens of a mouse that was serially inoculated with tumor cells from the adrenal gland of the first transplanted mouse. The mice were killed on days 63 and 83 after transplantation. (a) The images shown are from a mouse killed on day 63, as in (**B**). Original magnification ×100, Olympus BX51 N-34. The human/mouse chimerism of each organ was determined by analysis of human and mouse CD45 (b). For (**B**–**D**), each point of the chimerism data represents the mean value taken from two mice, with error bars indicating the s.e.m.
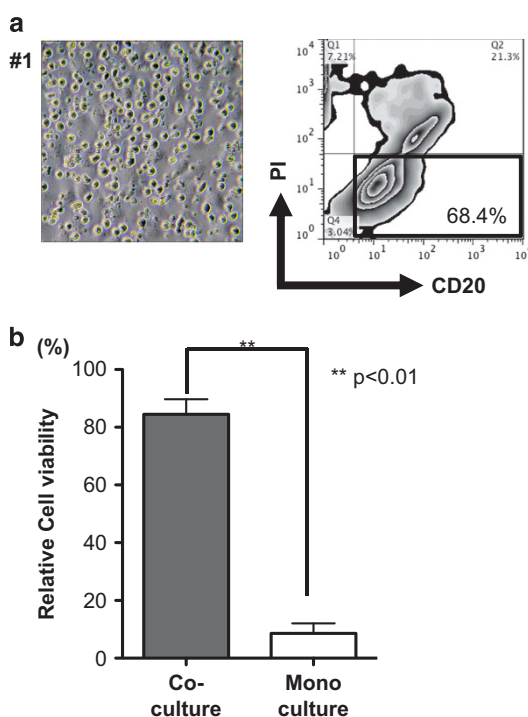
Figure 6. Dependency of tumor cells on HUVECs for survival. (**a**) Phase-contrast image of tumor cells on HUVECs 24 h after initiation of the co-culture (left panel) and a representative plot of FCM analysis of the survival of tumor cells co-cultured with HUVECs (right panel) are shown. (**b**) A bar graph showing relative cell viability of tumor cells in co-culture with HUVECs and tumor cells in monoculture. One hundred represents the percentage of viable cells at the start of the experiment. Each point represents the mean value taken from two representative independent experiments, with error bars indicating the s.e.m.

abnormalities. In array CGH analyses, persistent genomic copy number losses located on the chromosomal locations 6q21, 6q23-24 and 9p21 were detected (Figure 7A). We then analyzed the copy number of PRDM1, FOXO3, PERP and CDKN2A, which are located on common genomic copy number alterations loci, using genomic copy number real-time quantitative PCR. Copy number losses of PERP and CDKN2A were detected in tumor cells from all four mice by real-time quantitative PCR. Copy number losses of PRDM1 and FOXO3 were also detected in tumors 1 to 3 (Supplementary Figure S6). As genomic copy number alterations of PRDM1 and CDKN2A are known to occur in activated B-cell (ABC)-type diffuse large B-cell lymphoma (DLBCL),[27] we compared the pattern of genomic copy number alterations of IVLBCL with that of *bona fide* DLBCL using published data.[28] As expected, this comparison indicated that the copy number alterations of IVLBCL demonstrated similarity with the ABC type of DLBCL (Supplementary Figure S7). Moreover, comparison of the genomic DNA of various organs including the spleen, kidney, BM and adrenal gland from the same second transplanted mouse 3 revealed a difference in genomic copy number alterations on chromosomes 12, 21 and X loci (Figure 7B).

Subsequently, we performed GEP analyses of all tumors from all four mice. The gene expression of peripheral blood B cells used as a normal reference was homogenous, whereas that of IVLBCL tumors was apparently heterogeneous (Figure 7Ca). Clustering analysis also showed that tumor 1 was classified into a different cluster from that into which tumors 2 to 4 were classified (Figure 7Cb). We also compared tumor cells of IVLBCL with DLBCL. In this analysis using published data,[29] IVLBCL were clustered into

ABC-like DLBCL (Supplementary Figure S8). As significance analysis of microarray methods revealed overexpression or suppression of various genes including various oncogenes in the tumor cells (Supplementary Tables S3 and S4), we performed GSEA analyses to further analyze such gene expression. As shown in Figures 7D and E and Supplementary Table S5, GSEA analyses demonstrated that the chromosome 6p22 gene set that includes oncogenic transcription factor E2F3 was significantly enriched at a false discovery rate q-value of < 0.001 in tumor cells. Moreover, GSEA analyses also demonstrated that the Myosin pathway, which is related to the process of cell migration and actin reorganization, was significantly enriched at a false discovery rate q-value of 0.016 in normal B cells. These combined data indicated that the suppression of genes associated with cell migration might be related to IVLBCL pathogenesis.

DISCUSSION

We developed IVLBCL xenograft mouse models that originated from primary tumor cells of patients with IVLBCL, and used these mice to try to uncover the underlying biology of IVLBCL. The tumor cells from all four patients with IVLBCL retained the main characteristic of this disease, that is, the tumor cells lodged in vessels and sinusoids in all of the xenograft models. In addition, the tumor cells, at least in part, demonstrated survival dependency on vascular endothelial cells *in vitro*. These findings suggested that vascular and sinusoidal endothelial cells might play an important role as niches for IVLBCL tumors. Moreover, array CGH and GEP analyses indicated that there was a high likelihood that IVLBCL was classified into ABC-type DLBCL.[27,29]

In the present analyses, IVLBCL tumor cells, at least in part, displayed an *in vitro* survival dependency on HUVECs. According to the time-lapse engraftment analysis after inoculation of tumor cells, the transplanted tumor cells were engrafted and had initiated proliferation within the vessels and sinusoids of the liver by 1 week after inoculation. Moreover, serial passage of the tumor cells engrafted in various organs showed that tumor cells engrafted in the mouse adrenal gland mainly developed tumors in the adrenal gland of subsequently transplanted mice. These data suggested that IVLBCL tumor cells proliferate on vascular or sinusoidal endothelial cells that function as a niche, and that only tumor cells that are biologically adapted to an organ-specific niche can proliferate in that specific organ. In addition, array CGH data suggested the presence of different tumor clones among organs of the same mouse. The combined data suggested that tumor cells might be selected and/or clonally evolved to develop the disease in a specific organ.

GEP analysis demonstrated suppression of the Myosin pathway and other gene sets including ITGAL, associated with actin reorganization and/or cell migration.[30,31] Considering the heterogeneity of IVLBCL tumor cells in principal component analysis, the various alterations in cell surface and/or intracellular molecules related to cell migration might result in the inhibition of tumor cell migration and accordingly retain the tumor cells within the vessels or sinusoids in IVLBCL. Thus, a combination of tumor survival dependency on vascular and sinusoidal endothelial cells and inhibition of cell migration might evoke the specific disease phenotype of IVLBCL.

In the present analysis, we demonstrate that IVLBCL tumor cells have a memory B-cell phenotype in terms of cell surface antigens, and that the immunophenotypes are classified into the non-germinal center B cell-type DLBCL according to Hans' criteria.[26] Moreover, the genomic alterations and GEP data of the tumor cells are coincident with the characteristics of ABC-type DLBCL. These findings suggest that IVLBCL are likely to have originated from memory B cells as previously considered.[1]

In the present study, by the development and analyses of xenograft models we were able to uncover part of the veiled

pathogenesis of IVLBCL, and make interesting deductions regarding the disease mechanism. We believe that these models are an essential tool for understanding IVLBCL biology. However, careful interpretation of potential clonal selection and/or evolution of patient tumor cells during the development of the mouse models is required. In addition, we showed mutual interaction between
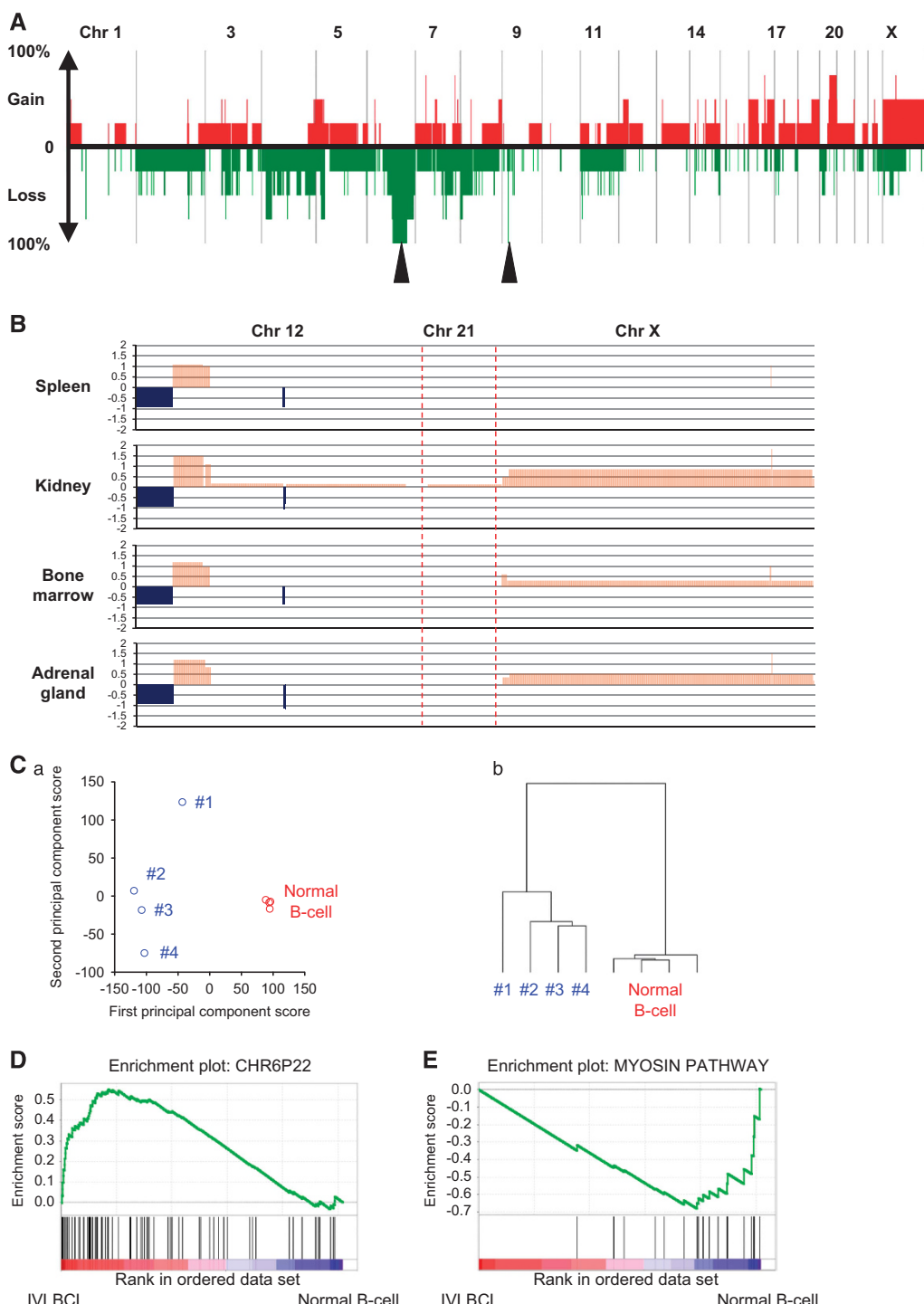

Figure 7. Array CGH analyses and GEP analyses of the IVLBCL tumor cells. (**A**) Copy number alterations in IVLBCL tumor cells from tumors formed in the spleen of all four mouse models are shown. Common copy number alterations that were detected on 6q21, 6q23-24 and 9p21 loci are indicated by black arrowheads. The x axis represents chromosomal regions and the y axis represents frequencies of gain (above 0) or loss (below 0). (**B**) Copy number alterations in the spleen, kidney, BM and adrenal gland from the same second transplanted mouse 3 are shown. Differences between organs in copy number alterations on Chr 12, Chr21 and Chr X were detected. (**C**) Principal component analysis (PCA) of IVLBCL tumors and control normal peripheral blood mononuclear cells (PBMCs) (a). Hierarchical clustering of the tumors from the four model mice and control normal PBMCs (b). (**D**) GSEA analyses indicated that the chromosome 6p22 gene set was significantly enriched for IVL tumors. (**E**) GSEA analysis indicated that the Myosin pathway gene set was significantly enriched for normal B cells.

IVLBCL tumor cells and vascular and sinusoidal endothelial cells *in vivo*. Careful interpretation of these data is also required in terms of the substantial difference between human and mouse stromal cells. Moreover, we compared IVLBCL tumor cells with peripheral B cells from healthy volunteer donor using GSEA analysis. We also compared tumor cells with DLBCL using published data that were derived using platform and labeling methods that differed from those that we used, as we could not find appropriate data in the public database. Careful interpretation of these data and future investigations are warranted to validate our results. Nevertheless, even considering the limitations of this study, by overcoming the difficulties of obtaining live tumor cells, the present analysis opens the door to uncovering the underlying biology of IVLBCL, and the obtained data should be meaningful in terms of the first elucidation of part of the disease mechanisms of IVLBCL.

AUTHOR CONTRIBUTIONS

K Shimada, TN, FH, M Seto, AT and HK designed research; K Shimada, K Sugimoto, TT, YT, AS and TA established mouse models; K Shimada, SS, K Sugimoto and YT performed experiments; K Shimada, MN, M Suguro, AH, IT, SN and M Seto analyzed and interpreted data; K Shimada, MN, M Suguro, AH, TDH and IT performed statistical analysis; TN, SN, FH, M Seto, AT and HK supervised research; K Shimada, MN, M Suguro, AH, IT, M Seto, AT and HK wrote the manuscript; and all authors reviewed and revised the manuscript.

REFERENCES

1 Nakamura S, Ponzoni M, Campo E. Intravascular large B-cell lymphoma. In: Swerdlow SH, Campo E, Harris NL, Jaffe ES, Pileri SA, Stein H *et al.* (eds), *WHO Classification of Tumours of Haematopoietic and Lymphoid Tissues*. IARC Press: Lyon, France, 2008; pp 252–253.

2 Ponzoni M, Ferreri AJ, Campo E, Facchetti F, Mazzucchelli L, Yoshino T *et al.* Definition, diagnosis, and management of intravascular large B-cell lymphoma:

proposals and perspectives from an international consensus meeting. *J Clin Oncol* 2007; **25**: 3168–3173.

3 Ferreri AJ, Campo E, Ambrosetti A, Ilariucci F, Seymour JF, Willemze R *et al.* Anthracycline-based chemotherapy as primary treatment for intravascular lymphoma. *Ann Oncol* 2004; **15**: 1215–1221.

4 Murase T, Yamaguchi M, Suzuki R, Okamoto M, Sato Y, Tamaru J *et al.* Intravascular large B-cell lymphoma (IVLBCL): a clinicopathologic study of 96 cases with special reference to the immunophenotypic heterogeneity of CD5. *Blood* 2007; **109**: 478–485.

5 Gill S, Melosky B, Haley L, ChanYan C. Use of random skin biopsy to diagnose intravascular lymphoma presenting as fever of unknown origin. *Am J Med* 2003; **114**: 56–58.

6 Asada N, Odawara J, Kimura S, Aoki T, Kamakura M, Takeuchi M *et al.* Use of random skin biopsy for diagnosis of intravascular large B-cell lymphoma. *Mayo Clin Proc* 2007; **82**: 1525–1527.

7 Matsue K, Asada N, Odawara J, Aoki T, Kimura S, Iwama K *et al.* Random skin biopsy and bone marrow biopsy for diagnosis of intravascular large B cell lymphoma. *Ann Hematol* 2011; **90**: 417–421.

8 Shimada K, Matsue K, Yamamoto K, Murase T, Ichikawa N, Okamoto M *et al.* Retrospective analysis of intravascular large B-cell lymphoma treated with rituximab-containing chemotherapy as reported by the IVL study group in Japan. *J Clin Oncol* 2008; **26**: 3189–3195.

9 Ferreri AJ, Dognini GP, Bairey O, Szomor A, Montalban C, Horvath B *et al.* The addition of rituximab to anthracycline-based chemotherapy significantly improves outcome in 'Western' patients with intravascular large B-cell lymphoma. *Br J Haematol* 2008; **143**: 253–257.

10 Shimada K, Kinoshita T, Naoe T, Nakamura S. Presentation and management of intravascular large B-cell lymphoma. *Lancet Oncol* 2009; **10**: 895–902.

11 Ponzoni M, Arrigoni G, Gould VE, Del Curto B, Maggioni M, Scapinello A *et al.* Lack of CD 29 (beta1 integrin) and CD 54 (ICAM-1) adhesion molecules in intravascular lymphomatosis. *Hum Pathol* 2000; **31**: 220–226.

12 Kusaba T, Hatta T, Tanda S, Kameyama H, Tamagaki K, Okigaki M *et al.* Histological analysis on adhesive molecules of renal intravascular large B cell lymphoma treated with CHOP chemotherapy and rituximab. *Clin Nephrol* 2006; **65**: 222–226.

13 Morton CL, Houghton PJ. Establishment of human tumor xenografts in immunodeficient mice. *Nat Protoc* 2007; **2**: 247–250.

14 Tomita N, Hiraga J, Kiyoi H, Ninomiya M, Sugimoto T, Ito M *et al.* Epigenetic regulation of CD20 protein expression in a novel B-cell lymphoma cell line, RRBL1, established from a patient treated repeatedly with rituximab-containing chemotherapy. *Int J Hematol* 2007; **86**: 49–57.

15 Dewan MZ, Watanabe M, Ahmed S, Terashima K, Horiuchi S, Sata T *et al.* Hodgkin's lymphoma cells are efficiently engrafted and tumor marker CD30 is expressed with constitutive nuclear factor-kappaB activity in unconditioned NOD/SCID/gammac(null) mice. *Cancer Sci* 2005; **96**: 466–473.

16 Ito M, Hiramatsu H, Kobayashi K, Suzue K, Kawahata M, Hioki K *et al.* NOD/SCID/gamma(c)(null) mouse: an excellent recipient mouse model for engraftment of human cells. *Blood* 2002; **100**: 3175–3182.

17 Ninomiya M, Abe A, Katsumi A, Xu J, Ito M, Arai F *et al.* Homing, proliferation and survival sites of human leukemia cells in vivo in immunodeficient mice. *Leukemia* 2007; **21**: 136–142.

18 van Dongen JJ, Langerak AW, Bruggemann M, Evans PA, Hummel M, Lavender FL *et al.* Design and standardization of PCR primers and protocols for detection of clonal immunoglobulin and T-cell receptor gene recombinations in suspect lymphoproliferations: report of the BIOMED-2 Concerted Action BMH4-CT98-3936. *Leukemia* 2003; **17**: 2257–2317.

19 Katakai T, Hara T, Sugai M, Gonda H, Shimizu A. Lymph node fibroblastic reticular cells construct the stromal reticulum via contact with lymphocytes. *J Exp Med* 2004; **200**: 783–795.

20 Tagawa H, Tsuzuki S, Suzuki R, Karnan S, Ota A, Kameoka Y *et al.* Genome-wide array-based comparative genomic hybridization of diffuse large B-cell lymphoma: comparison between CD5-positive and CD5-negative cases. *Cancer Res* 2004; **64**: 5948–5955.

21 Hocking TD, Boeva V, Rigaill G, Schleiermacher G, Janoueix-Lerosey I, Delattre O *et al.* SegAnnDB: interactive Web-based genomic segmentation. *Bioinformatics* 2014; **30**: 1539–1546.

22 Eisen MB, Spellman PT, Brown PO, Botstein D. Cluster analysis and display of genome-wide expression patterns. *Proc Natl Acad Sci USA* 1998; **95**: 14863–14868.

23 Tusher VG, Tibshirani R, Chu G. Significance analysis of microarrays applied to the ionizing radiation response. *Proc Natl Acad Sci USA* 2001; **98**: 5116–5121.

24 Subramanian A, Tamayo P, Mootha VK, Mukherjee S, Ebert BL, Gillette MA *et al.* Gene set enrichment analysis: a knowledge-based approach for

interpreting genome-wide expression profiles. *Proc Natl Acad Sci USA* 2005; **102**: 15545–15550.

25 Murase T, Nakamura S, Kawauchi K, Matsuzaki H, Sakai C, Inaba T *et al.* An Asian variant of intravascular large B-cell lymphoma: clinical, pathological and cytogenetic approaches to diffuse large B-cell lymphoma associated with haemophagocytic syndrome. *Br J Haematol* 2000; **111**: 826–834.

26 Hans CP, Weisenburger DD, Greiner TC, Gascoyne RD, Delabie J, Ott G *et al.* Confirmation of the molecular classification of diffuse large B-cell lymphoma by immunohistochemistry using a tissue microarray. *Blood* 2004; **103**: 275–282.

27 Alizadeh AA, Eisen MB, Davis RE, Ma C, Lossos IS, Rosenwald A *et al.* Distinct types of diffuse large B-cell lymphoma identified by gene expression profiling. *Nature* 2000; **403**: 503–511.

28 Suguro M, Yoshida N, Umino A, Kato H, Tagawa H, Nakagawa M *et al.* Clonal heterogeneity of lymphoid malignancies correlates with poor prognosis. *Cancer Sci* 2014; **105**: 897–904.

29 Rosenwald A, Wright G, Chan WC, Connors JM, Campo E, Fisher RI *et al.* The use of molecular profiling to predict survival after chemotherapy for diffuse large-B-cell lymphoma. *N Engl J Med* 2002; **346**: 1937–1947.

30 Vicente-Manzanares M, Ma X, Adelstein RS, Horwitz AR. Non-muscle myosin II takes centre stage in cell adhesion and migration. *Nat Rev Mol Cell Biol* 2009; **10**: 778–790.

31 Maekawa M, Ishizaki T, Boku S, Watanabe N, Fujita A, Iwamatsu A *et al.* Signaling from Rho to the actin cytoskeleton through protein kinases ROCK and LIM-kinase. *Science* 1999; **285**: 895–898.